J Nanotechnol Nanomaterials. 2025;6(1):76–88.

Journal of Nanotechnology and Nanomaterials Original Research

Enhancing p-type DSSC Performance through Nio-carbon Allotrope Hybrids: A Study of Functionalized MWCNT Integration

Chivukula Narayana Murthy[1,*]

[1]Department of Applied Chemistry, Faculty of Technology & Engineering, The Maharaja Sayajirao University of Baroda, Vadodara-390001, India

[*]Correspondence should be addressed to Chivukula Narayana Murthy, chivukula_mn@yahoo.com

Received date: May 24, 2025, **Accepted date:** July 08, 2025

Citation: Murthy CN. Enhancing p-type DSSC Performance through Nio-carbon Allotrope Hybrids: A Study of Functionalized MWCNT Integration. J Nanotechnol Nanomaterials. 2025;6(1):76-88.

Abstract

In this study, we systematically investigated the influence of various carbon allotropes on the photovoltaic performance of p-type dye-sensitized solar cells (DSSCs) using nickel oxide (NiO) nanotubes as the base semiconductor. The selected carbon nanostructures multi-walled carbon nanotubes (MWCNTs), reduced graphene oxide (RGO), graphene quantum dots (GQDs), and fullerenes (C_{60}) were integrated with NiO and evaluated based on their structural and electrochemical characteristics. The resulting NiO-based nanohybrids exhibited a trend in power conversion efficiency (PCE) as follows: NiO@GQD (NG) < NiO@C_{60} (NF) < NiO@RGO (NR) < NiO@f-MWCNT (NM), with PCE values of 0.55%, 0.60%, 0.72%, and 0.80%, respectively. Among all NM nanohybrids exhibited the highest performance, with a short-circuit current density (Jsc) of 2.53 mA cm^{-2}, an open-circuit voltage (Voc) of 0.56 V, and a fill factor (FF) of 56.46%. The superior performance of the NM device is attributed to enhanced dye adsorption and efficient charge transfer facilitated by the functionalized MWCNT network. To further explore its potential, the NM nanohybrid was strategically incorporated into an n-type DSSC by integrating it with a TiO_2 active layer. This ternary NiO@f-MWCNT/TiO_2 composite was synthesized with varying MWCNT loadings (10–50 wt %). The TiO_2+NM20 photoanode exhibited the highest PCE of 6.50%, marking a 34% improvement over the bare TiO_2 device. This enhancement is credited to improved light absorption, reduced internal resistance, and the excellent charge transport properties.

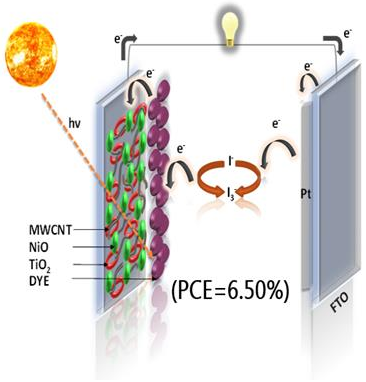

Keywords: NiO, Nanohybrids, p- type, DSSC, Nanomaterial

Introduction

DSSCs are low-cost, eco-friendly solar cells offering a flexible alternative to silicon-based photovoltaics [1,2]. Photoanode plays a critical role in determining the efficiency of the device, with its performance influenced by light harvesting efficiency, electron injection, and recombination rates [2,3]. In n-type DSSCs, semiconducting oxides such as TiO_2 and ZnO are commonly used as photoanode materials. However, for p-type DSSCs, which operate via hole transport

instead of electron transport, NiO nanotubes is one of the most promising candidates. NiO is a wide bandgap (3.5–4.0 eV) semiconductor that exhibits good chemical stability, resistance to photo corrosion, and excellent electronic properties [4–6]. It acts as an effective blocking layer, minimizing recombination losses, and also provides a suitable pathway for hole injection and transport. In recent years, significant research efforts have focused on improving the PCE of DSSCs through modifications in the photoanode material [7–9]. These modifications include incorporating carbon-based materials such as graphene quantum dots (GQDs) [10], reduced graphene oxide (RGO) [8], fullerenes (C_{60}) [7], and multi-walled carbon nanotubes (MWCNTs) [6], either as additives or as hybrid structures with metal oxides. These carbon allotropes offer several advantages due to their high surface area, electrical conductivity, chemical stability, and excellent optoelectronic properties. Their extended π-conjugation systems enable efficient charge transport, while their structural versatility allows for integration in various device architectures [10,11]. RGO is obtained by reducing of graphene oxide to enhance conductivity via restored sp^2 domains. GQDs, as 0D fragments, exhibit tunable optical and electronic properties due to quantum confinement. MWCNT offer high surface area, superior electrical conductivity, and mechanical strength, making them ideal for DSSC applications [6–8]. Carbon allotropes have been widely studied in n-type DSSCs, their integration with p-type systems, especially with NiO, remains relatively unexplored. While some studies have investigated binary composites like NiO-MWCNT [9], NiO-RGO [12], NiO GQD [13], and NiO-fullerene [7], a comprehensive comparative study combining NiO nanotubes with all these carbon allotropes in DSSC before this has not yet been reported. NiO@f-MWCNT, NiO@GQD, NiO@RGO, and NiO@fullerene, designed for p-type DSSC photoanodes [14]. These hybrids were synthesized and characterized for their structural, morphological, optical, and electrochemical properties. Here, NM hybrid showed superior performance, attributed to enhanced charge transport, reduced recombination, and improved light harvesting due to the synergistic interaction between NiO and the functionalized carbon nanotubes. To further explore the hybrid potential of NiO and f-MWCNT, we fabricated a novel ternary composite system NiO/f-MWCNT/TiO_2 for DSSC photoanodes. Initially, NiO nanotubes were synthesized using the sol-gel method. f-MWCNT interaction with NiO and TiO_2 matrices. Different photoanodes were prepared by varying the concentration of f-MWCNTs from 10% to 50% in the composite (NM10–NM50/TiO_2) [6]. This ternary system demonstrated significant improvement in photovoltaic performance. The bare TiO_2 based DSSC showed a PCE of 4.85%, while the optimized NM20/TiO_2 system achieved a PCE of 6.50%, indicating an approximate 34% enhancement. This improvement is attributed to the effective electron collection and transport facilitated by f-MWCNTs, combined with NiO's blocking capability and TiO_2's role as an electron acceptor. Overall, this study highlights the advantages of f-MWCNTs with NiO for enhancing the performance of p-type DSSCs i.e. NM nanocomposite. The successful integration of NM with TiO_2 further emphasizes the potential of such ternary systems in overcoming limitations of conventional photoanodes. These findings pave the way for future research into advanced hybrid structures for efficient, low-cost, and sustainable solar energy devices.

Materials and Methods

All chemicals were of analytical grade and used without further purification. Solvents were freshly distilled prior to use.

Chemicals and reagents

Nickel nitrate hexahydrate ($Ni(NO_3)_2{\cdot}6H_2O$), dimethylglyoxime (DMG), multi-walled carbon nanotubes (MWCNTs, 98%, OD: 10–20 nm, length: 0.5–500 nm), graphene powder, fullerene (C_{60}), and meta-chloroperbenzoic acid (MCPBA) were procured from Sigma-Aldrich (USA). Nitric acid (HNO_3, 67%), sulfuric acid (H_2SO_4), sodium hydroxide (NaOH), phosphoric acid (H_3PO_4), dimethylformamide (DMF), potassium permanganate ($KMnO_4$), hydrogen peroxide (H_2O_2), hydrochloric acid (HCl), ethanol (C_2H_5OH), and citric acid were obtained from Fisher Scientific. N719 dye was purchased from TCI Chemicals and used as received. Fluorine-doped tin oxide (FTO) coated glass substrates (TCO22-15, sheet resistance: 15 Ω cm^{-2}) were sourced from Solaronix (Switzerland).

Synthesis of NiO Nanotubes

A 0.1 M ethanolic solution of DMG was added dropwise to a 0.1 M aqueous solution of $Ni(NO_3)_2{\cdot}6H_2O$ under continuous stirring at room temperature. The reaction mixture was stirred for 6 hours, resulting in a homogeneous solution. The precipitate was collected, washed with ethanol and distilled water, and dried at 80°C for 5 hours. Subsequently, it was calcinated at 450°C for 2 hours to obtain NiO nanotubes [15].

Functionalization of MWCNTs

1 g of MWCNTs was treated with a 3:1 mixture of concentrated H_2SO_4 and HNO_3. The mixture was sonicated for 30 minutes at room temperature and then refluxed at 60°C for 8 hours. Post-reaction, the mixture was neutralized, washed with distilled water, and dried in a vacuum oven at 100°C to yield f-MWCNTs [16].

Synthesis of RGO

RGO was synthesized using an improved Hummer's method. Graphite flakes (3 g) and $KMnO_4$ (18 g) were added to a

mixture of concentrated H_2SO_4 and H_3PO_4 (9:1, 360:40 mL). The reaction mixture was stirred at 50°C for 12 hours. After cooling to room temperature, it was poured onto ice containing 30% H_2O_2. The resultant mixture was filtered, and the filtrate was centrifuged at 4,000 rpm for 4 hours. The solid residue was washed sequentially with water, 30% HCl, and ethanol, then vacuum-dried overnight to obtain RGO [8].

Synthesis of GQDs

Citric acid (2.0 g) was heated in a 250 mL three-necked flask at 150 °C until the solution turned orange-red, indicating pyrolysis. A 1.5 M NaOH solution was then added dropwise until the pH reached 7.0. The resulting solution was diluted to 100 mL and stored at 4 °C to obtain GQDs [17].

Functionalization of fullerene

MCPBA (4 g) was dissolved in 200 mL of benzene, followed by the addition of fullerene (120 mg). The mixture was refluxed at 60°C for 6 hours. After solvent evaporation at 80°C, a dark brown precipitate formed, which was washed with water and ethanol, then dried at 50°C to yield oxidized fullerene [18].

Synthesis of NiO carbon allotrope hybrids

For the synthesis of NiO-carbon allotropes hybrid, a stoichiometric ratio of 1:0.2 between nickel oxide (NiO) and carbon allotropes (including f-MWCNT, GQD, RGO, and fullerene for the respective NiO-f-MWCNT, NiO-GQD, NiO-RGO, NiO-fullerene nano-hybrids) was employed. The total mass of the materials was introduced into a 100 ml solution of DMF, and the mixture underwent ultrasonication for 10 minutes to ensure homogeneity. Following ultrasonication, the prepared mixture was subjected to reflux conditions for 12 hours at a temperature of 80°C. Subsequently, the reaction mixture was heated to 80°C to induce the evaporation of the solvent. The final product obtained was a dark grey-colored solid, representing the NiO-carbon allotropes hybrid [14].

NM nanocomposites,

NM composites were prepared by *in-situ* precipitation method. NiO:f-MWCNTs were taken in a ratio of 1:0.1, 1:0.2, 1:0.3, 1:0.4, and 1:0.5 respectively, and dispersed in 50 ml of isopropyl alcohol. After that, the dispersion was sonicated for 30 min to form a homogenous solution. The reaction was refluxed at 50°C for 5 h. After completion, the black precipitates were washed and filtered with distilled water. Subsequently, they were dried under vacuum at 80°C for 12 h. Finally, NM of 10%, 20%, 30%, 40%, and 50% nanocomposites were prepared and coded as NM10, NM20, NM30, NM40, and NM50 for device fabrication respectively [6].

Fabrication of DSSC

The nickel nitrate hexahydrate (0.8 M, 20 mL) precursor solution was prepared and stabilized with 2 drops of conc. Hydrochloric acid. The solution was stirred and heated at 40°C for 2 hours to get transparent solution. The precursor solution was spin coated on cleaned FTO glasses at 2,000 rpm for 60 sec. and then annealed at 450°C for 30 min. A thin film of prepared NiO and composites nano particles were prepared using doctor-blade method using Scotch tape as a spacer by forming NiO paste containing ethyl cellulose and α-terpinol. The prepared films were heated in the open furnace at 450°C for 30 min and soaked into dye solution (N719 dye, 10 mm) for 24 hours at room temperature. For ternary composite the on FTO TiO_2 nanoparticle (P25) mixed with NM composites layer spread followed by calcination at 450°C in open air. On the other hand, predrilled cleaned FTO glass electrodes were spin coated with H_2PtCl_6 (platinic acid) solution at 2,000 rpm and calcined at 450°C for 30 min. The dye soaked NiO electrodes were assembled face to face with Pt coated electrode using 25 µm thick thermoplastic (Surlyn, Dyesol). The liquid electrolyte, containing 0.5 M LiI, 0.05 M I2, 0.5 M TBP in 3-methoxy propionitrile was introduced through predrilled hole in Pt electrode, which was sealed afterwards using epoxy adhesive and cover glass. The fabricated devices were stored under the dark at room temperature for 12 hours prior to photovoltaic measurements. The active area of the DSSC devices was strictly maintained to 0.25 cm^2.

Characterization techniques

The prepared nanocomposites were characterized by different techniques to investigate the chemical and physical properties of the nanocomposites. Fourier transform infrared spectroscopy (FTIR) characterization was carried out to examine the structural determination of composites using Shimadzu IR affinity 1S Spectrophotometer in the range of 4000–400 cm^{-1} on KBr pellet. Ultra-Violet Visible spectroscopy (UV–Vis) spectra of nanocomposites were recorded using a Hitachi U-2900 Spectrophotometer. X-ray diffraction powder (XRD) measurement of samples were per formed with a PAN Analytical Diffractometer model Imperial using CuKα radiation with a scanning speed of 10°/min and recorded in the 2Θ range of 10°–100°. Study of topography or surface morphology of nano composites were carried out by Scanning electron microscope (SEM, Carl Zeiss EVO 18) and Transmission electron microscopy (TEM) carried out using a JEOL (JEM-200 CX) (LEO-440) having accelerating voltage of 200 kV. The samples for TEM were prepared in isopropyl alcohol solvent. For the determination of surface chemical composition, an X-ray photoelectron spectrometer (XPS) with a radiation source of Al Kα (1486.7 eV) was

used. The electrochemical impedance spectroscopic (EIS) measurements were carried out using Solartron 1,260 gain phase analyzer along with Solartron 1287 electrochemical interface by sweeping the frequency from 1.2 MHz to 0.1 Hz with an AC amplitude of 10 mV with 0 V applied bias. The NiO-based composites were sandwiched between two platinum electrodes. The Mott-Schottky analysis were performed using three-electrode system. NiO-based composite-coated FTO glass was used as working Platinum wire as counter and saturated calomel electrode as reference electrode were taken with 0.1 N KCl as electrolyte. The slope and acceptor density values were calculated using our previous report [19]. The photovoltaic measurements (J-V) were performed using CHI660E electrochemical workstation (CH instruments, USA under the light illumination (Solar simulator, SS80 AAA, Photoemission Tech, USA) with light intensity of 100 mW cm^2 with AM 1.5 G. The open-circuit voltage decay (OCVD) spectra were measured using CHI660E upto 200 s after light cut off. The electro chemical impedance spectroscopy (EIS) measurements were measured by sweeping the frequency from 1.2 MHz to 0.1 Hz with an AC amplitude of 10 mV with –0.65 V applied bias using Solartron 1260 gain phase analyzer along with Solartron 1287 electrochemical interface under dark conditions. The incident photon to-current conversion efficiency (IPCE) of the devices was measured using IPCE system (Oriel IQE-200, Newport, USA) with 250 W quartz tungsten halogen (QTH) lamp as the light source.

Results and Discussion

Structural properties

FTIR spectroscopy: Figure 1 presents the FTIR spectra of the NM, NG, NR, and NF nanohybrids, revealing characteristic functional groups. For NM, peaks at 3,443 cm^{-1} and 1,747 cm^{-1} correspond to – OH and C=O stretching vibrations, respectively, while a band at 435 cm^{-1} indicates NiO [6,20]. The presence of asymmetric and symmetric C–H vibrations at defect sites of acid-treated MWCNTs further confirms methylene groups. In the NG nanohybrid, peaks at 3,438 cm^{-1} (– OH), 1,741 cm^{-1} (C=O), and 492 cm^{-1} (NiO) are observed, along with bands at 1,587, 1,386, and 1,109 cm^{-1} attributed to C=C, C–H, and C–O, respectively. Additional peaks at 2,921 and 2,850 cm^{-1} correspond to asymmetric and symmetric C–H stretching. The NR spectrum exhibits prominent peaks at 3,438 (–OH), 2,922 (–CH), 1,760 (C=O), 1,616 (C=C), 1,109 (C–O), and 440 cm^{-1} (NiO) [15]. For NF, the bands at 3,438, 2,922, and 2,854 cm^{-1} represent –OH and C–H stretching, while peaks at 1,750, 1,545, 1,382, 1,114, and 421 cm^{-1} are assigned to C=O, C=C, C–H, C–O, and NiO vibrations, respectively.

X-ray diffraction (XRD): XRD analysis (Figure 2) confirms the crystalline nature and phase purity of all NiO and NiO- based nanohybrids (NM, NG, NR, and NF). Distinct diffraction peaks at 25.75° correspond to the (002) plane of carbon materials [12,16], while peaks at 37.1°, 44.32°, 51.7°, 63.10°, 76.20°, and 79.52° are indexed to the (111), (200), (212), (220), (311), and (222) planes of cubic NiO, respectively [15]. In case of nano hybrids both carbon and NiO peaks present which verifies successful formation of NiO-carbon nanohybrids.

Raman spectroscopy: Raman spectra (Figure 3) exhibit characteristic D (~1,350 cm^{-1}) and G (~1,580 cm^{-1}) bands of carbon allotropes in all hybrids (NM, NG, NR, and NF), indicating structural defects and graphitic domains [8]. NiO-specific modes at 545, 780, and 1,094 cm^{-1} correspond to LO, 2TO, and 2LO phonon vibrations, respectively [15,19,21]. These combined signals confirm the coexistence of NiO and carbon phases in the nanohybrids.

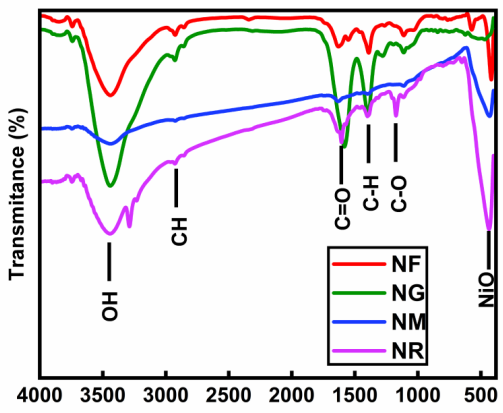

Figure 1. FTIR of NF, NG, NM and NR.

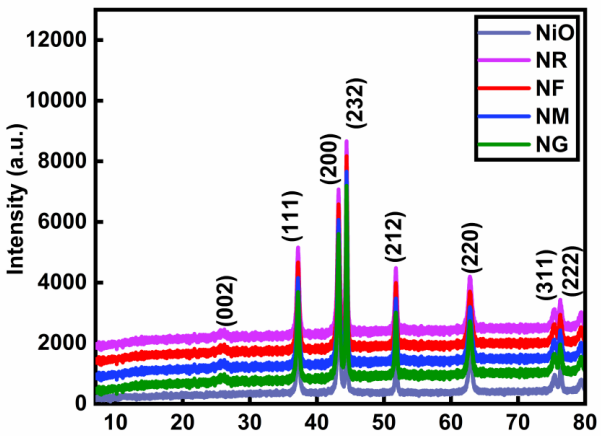

Figure 2. XRD of NiO, NF, NG, NM and NR.

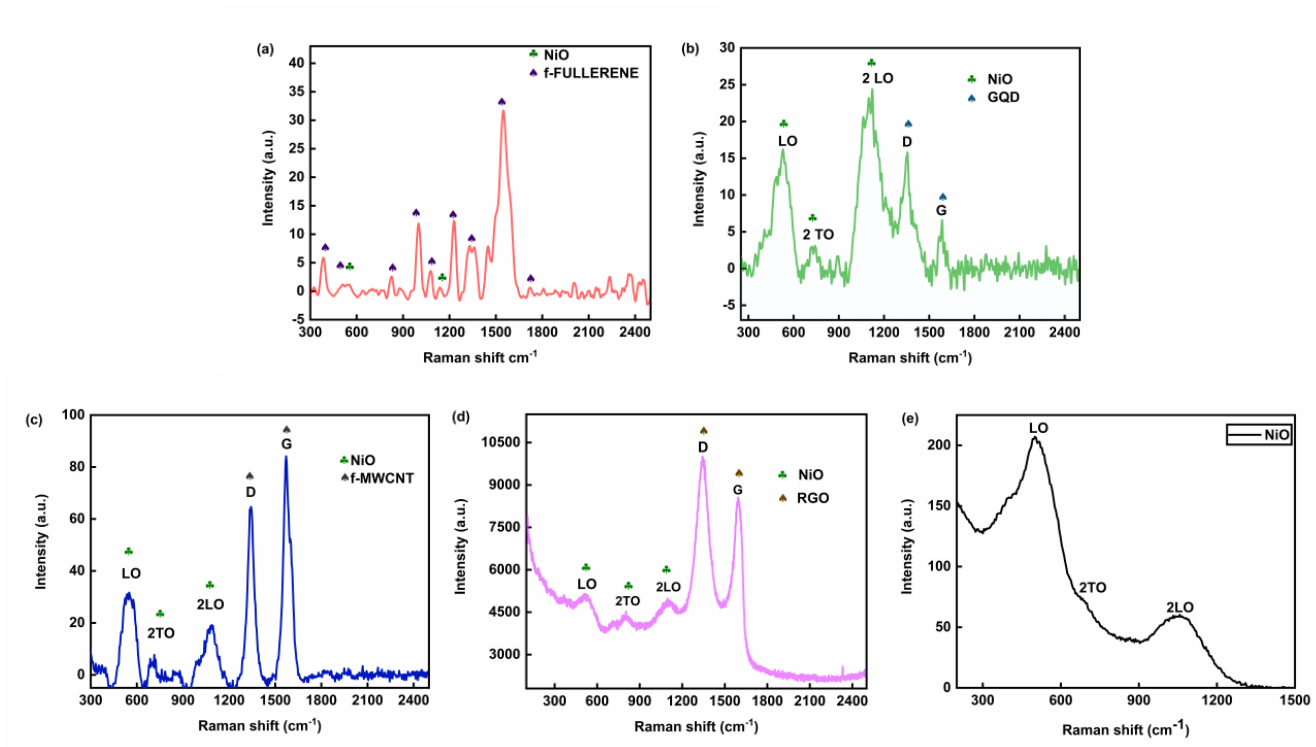

Figure 3. FTIR of NF, NG, NM, NR and NiO.

X-ray photoelectron spectroscopy (XPS): The elemental composition and oxidation states of the NF, NG, NM, and NR nanohybrids were investigated using X-ray photoelectron spectroscopy (XPS). The XPS results confirmed a similar elemental profile across all the nanohybrids. **Figures 4a–4d** shows the Ni 2p spectra, where distinct peaks at 851.1 and 852.8 eV correspond to the Ni $2p_3/_2$ region, confirming the presence of Ni^{2+} species. A peak observed at 869.7 eV is assigned to the Ni $2p_1/_2$ spin–orbit level, further validating the existence of NiO. Additionally, two prominent satellite peaks at 858.8 and 876.4 eV are characteristic of Ni^{2+} and serve as conclusive evidence for the formation of NiO shells in all nanohybrids [21].

The deconvoluted C 1s spectra, displayed in **Figures 6e–6h**, highlight the presence of various oxygen-containing

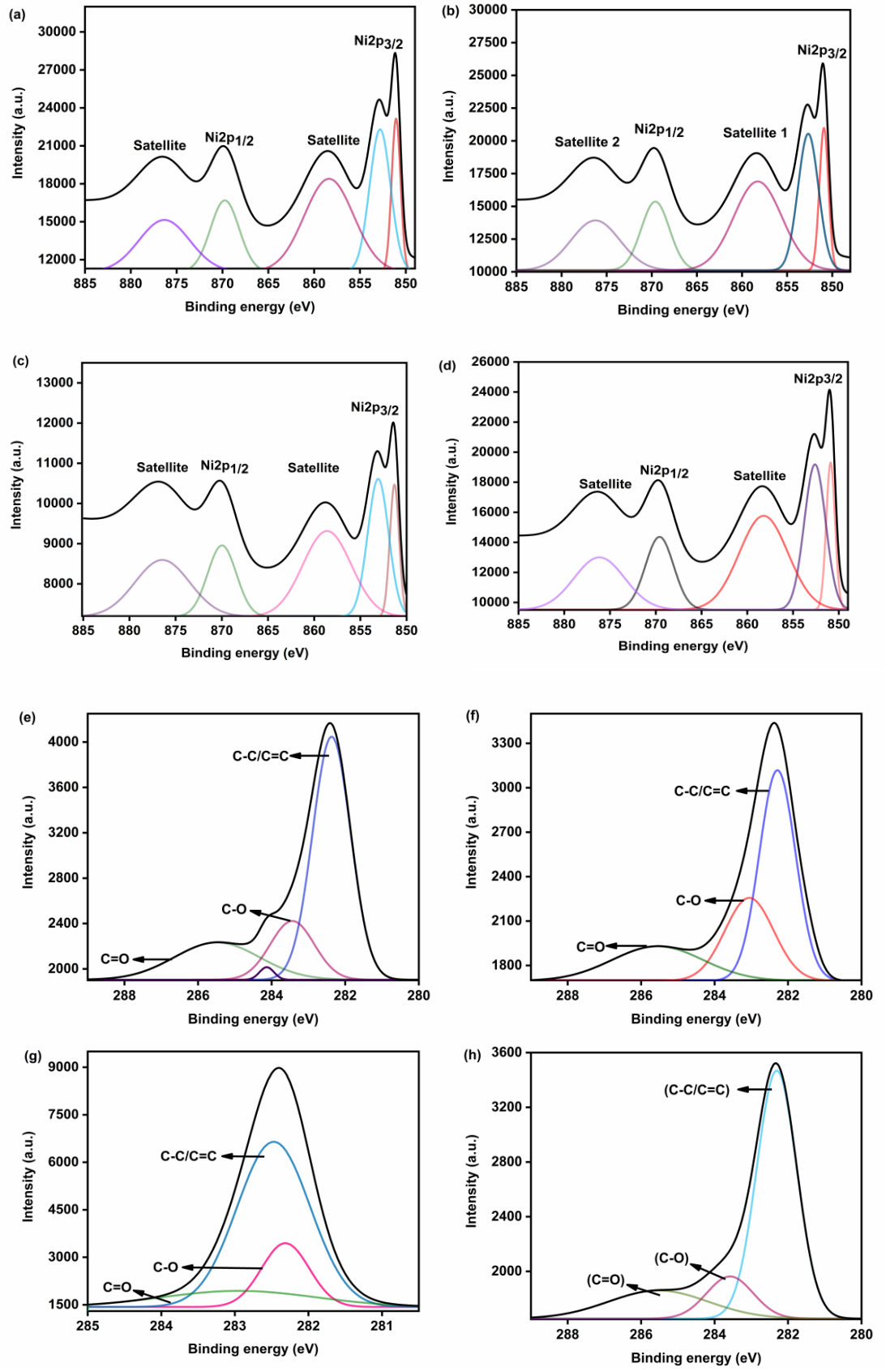
(a)
Satellite
Ni2p1/2
Satellite
Ni2p3/2
Intensity (a.u.)
Binding energy (eV)
(b)
Satellite 2
Ni2p1/2
Satellite 1
Ni2p3/2
Intensity (a.u.)
Binding energy (eV)
(c)
Satellite
Ni2p1/2
Satellite
Ni2p3/2
Intensity (a.u.)
Binding energy (eV)
(d)
Satellite
Ni2p1/2
Satellite
Ni2p3/2
Intensity (a.u.)
Binding energy (eV)
(e)
C-C/C=C
C-O
C=O
Intensity (a.u.)
Binding energy (eV)
(f)
C-C/C=C
C-O
C=O
Intensity (a.u.)
Binding energy (eV)
(g)
C-C/C=C
C-O
C=O
Intensity (a.u.)
Binding energy (eV)
(h)
(C-C/C=C)
(C-O)
(C=O)
Intensity (a.u.)
Binding energy (eV)

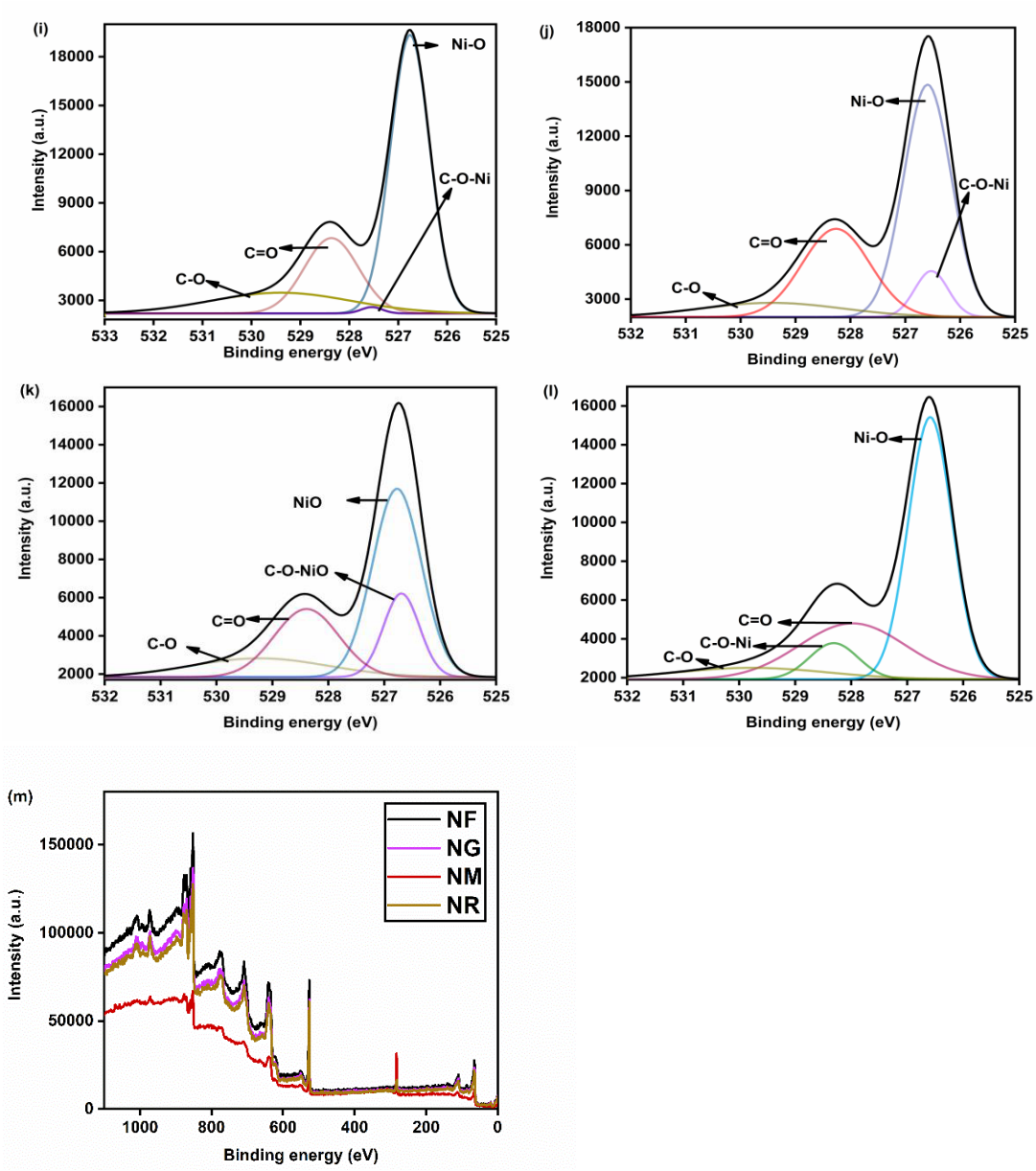

Figure 4. XPS analysis of Ni 2p of (**a**) NF, (**b**) NG, (**c**) NM, and (**d**) NR, (**e**) C 1s of NF, (**f**) NG, (**g**) NM, and (**h**) NR, (**i**) O 1s of NF, (**j**) NG, (**k**) NM, (**l**) NR, and (**m**) survey spectrum.

functional groups. A dominant peak at 282.30 eV corresponds to non-oxygenated, sp^2-hybridized carbon (C=C/C–C), which is typical of carbon allotropes. Additional peaks at 283.45 eV and 285.50 eV are assigned to C–O and C=O bonds, respectively, indicating surface oxygen functionalities present on the carbonaceous components [16,19,21]. **Figures 4i–4l** presents the O 1s spectra for all nanohybrids. A strong peak at 526.7 eV is attributed to lattice oxygen (O^{2-}) in NiO. Peaks at 528.7 and 529.5 eV correspond to oxygen atoms involved in C=O and C–O bonding, respectively. The appearance of an additional peak at 527.5 eV after the integration of NiO suggests the formation of C–O–Ni linkages. Finally, **Figure 4m** provides the survey spectra of the nanohybrids, clearly showing the presence of nickel, oxygen, and carbon. These results collectively confirm the successful formation of NiO-based carbon nanohybrids with chemically bonded components.

Transmission electron microscopy (TEM): In **Figure 5a**, the NiO sample exhibits a well-defined nanotubular morphology with an average diameter of approximately 0.15 µm. Minor agglomerations are observed, likely due to residual impurities or incomplete dispersion. **Figure 5b**

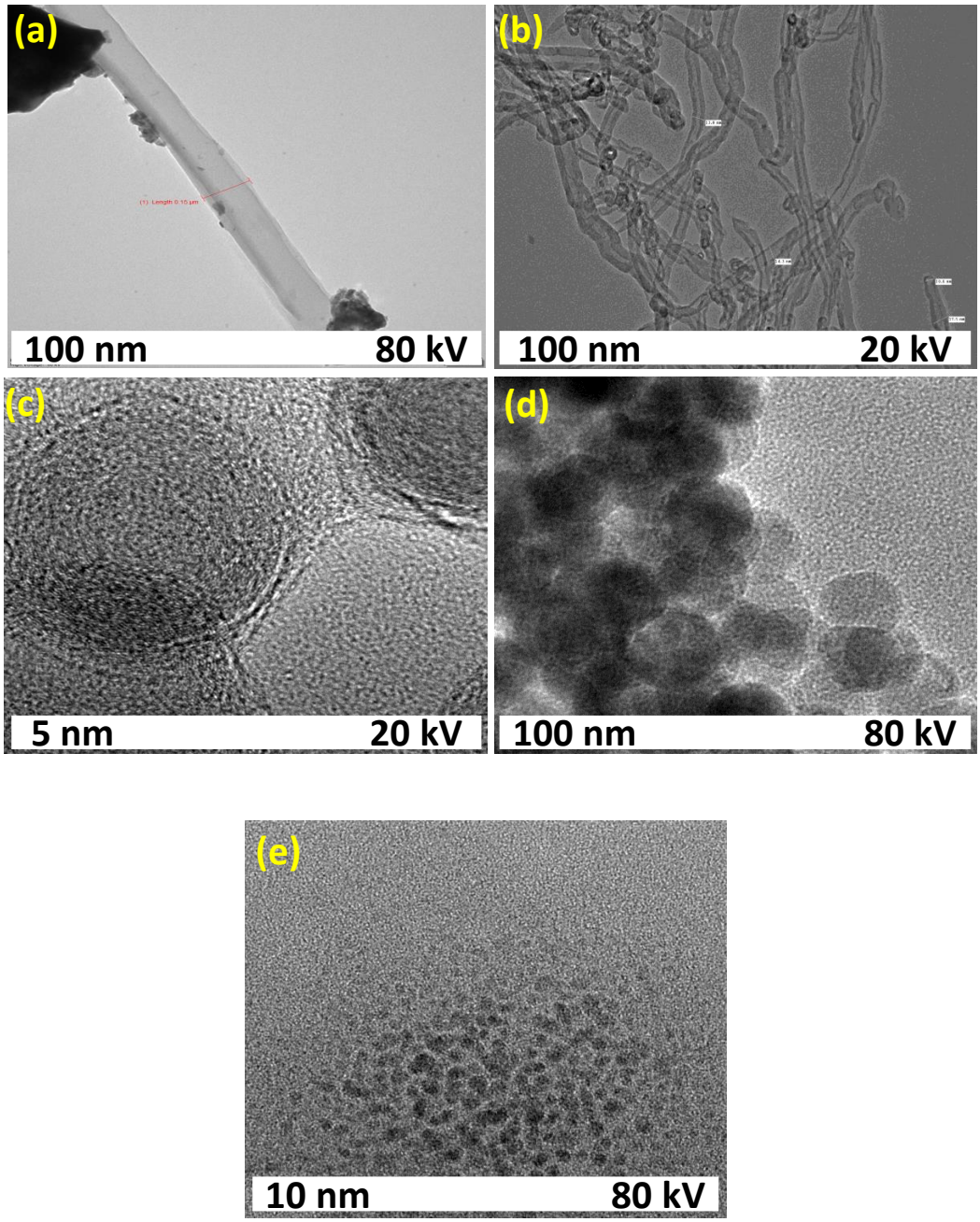

Figure 5. TEM of NiO nanotubes (**a**), f-MWCNT (**b**), RGO (**c**), fullerene (**d**) and GQD (**e**).

displays elongated, noodle-like structures characteristic of f-MWCNTs, with diameters ranging from 15 to 30 nm. **Figure 5c** reveals thin, wrinkled sheet-like structures of RGO, where the fringed edges confirm the exfoliated and layered morphology typical of RGO. **Figure 5d** shows uniformly distributed nanoparticles with spherical morphology, resembling fullerene-like structures. Finally, in **Figure 5e**, the GQDs appear as well-dispersed, nanoscale spherical entities, indicating successful synthesis with minimal aggregation.

Scanning electron microscopy (SEM): SEM was employed to examine the surface morphology and structural features of the synthesized materials. As depicted in **Figure 6a**, the NiO sample exhibits a well-defined nanotubular morphology, confirming the successful formation of tubular

structures. The f-MWCNT in **Figure 6b** reveals a characteristic noodle-like morphology, typical of functionalized multi-walled carbon nanotubes, which are well-integrated with NiO nanoparticles. **Figure 6c** illustrates, reduced graphene oxide exhibits an irregular, folded, and wrinkled sheet-like morphology. This structural deformation contributes to increased surface area and disorder, which can enhance charge transport properties in device applications. **Figure 6d** shows the fullerene, where the fullerene-based nanoparticles appear to adopt an elongated, rod-like morphology, suggesting possible aggregation or alignment during synthesis. Lastly, in **Figure 6e**, in the GQDs are observed as ultra-fine, uniformly distributed nanostructures with a rice-grain-like appearance, indicative of nanoscale dimensions and good dispersion.

Photovoltaic performance and electrochemical impedance spectroscopy (EIS)

To assess the photovoltaic behavior of the synthesized NiO-based nanohybrids, DSSCs were fabricated using N719 dye as the sensitizer. Devices incorporating four distinct nanohybrids NF, NG, NM, and NR were systematically compared to a reference device based on pristine NiO. All devices employed a standard liquid-state electrolyte. The J–V characteristics under AM 1.5 illumination are shown in **Figure 7a**, and the photovoltaic parameters including Jsc, Voc, fill factor FF, and PCE are compiled in **Table 1**.

The reference DSSC based on bare NiO exhibited poor performance, delivering only 0.17% efficiency with a low

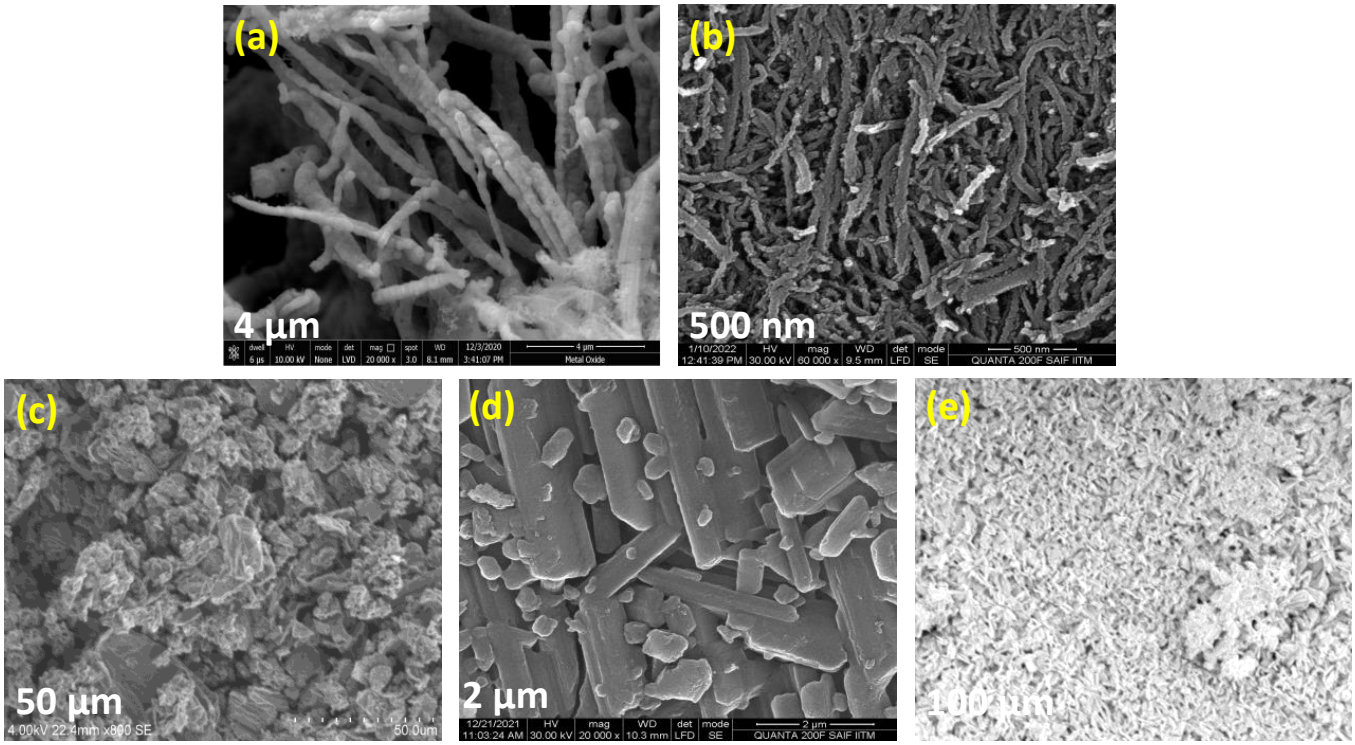

Figure 6. SEM of NiO nanotubes (**a**), f-MWCNT (**b**), RGO (**c**), fullerene (**d**) and GQD (**e**).

Table 1. Photovoltaic and electrochemical measurements.

Device	Jsc[a] (mA cm^{-2})	Voc[a] (V)	FF[a] (%)	η[a] (%)	Rct[b] (Ω)	Rrec[b] (Ω)
TiO_2	11.35	0.63	67.82	4.85	30.67	131.26
TiO_2 + NM10	13.07	0.66	66.30	5.72	29.36	146.32
TiO_2 + NM20	14.67	0.67	67.13	6.50	26.40	164.32
TiO_2 + NM30	13.84	0.67	36.41	5.88	26.82	148.65
TiO_2 + NM40	13.37	0.67	63.68	5.62	27.31	142.41
TiO_2 + NM50	13.20	0.66	64.27	5.60	27.44	139.11

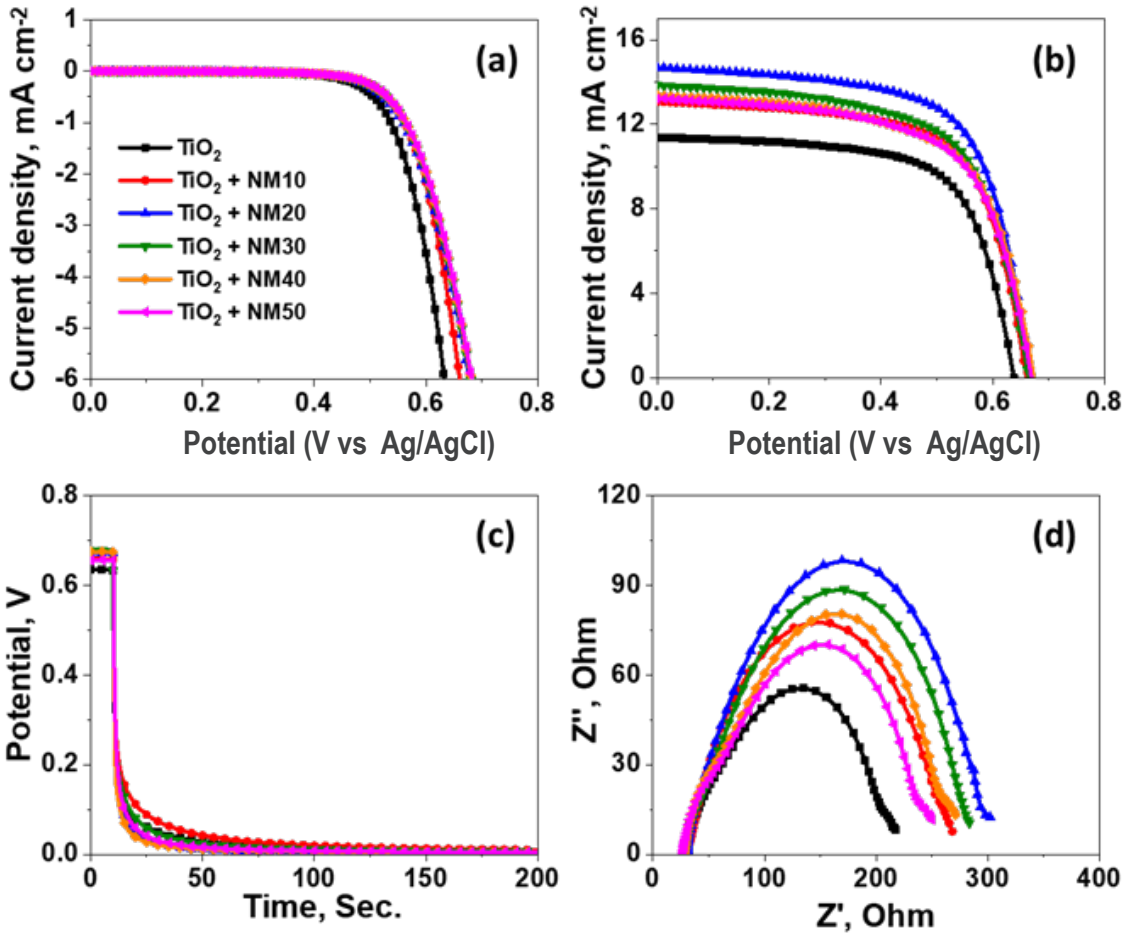

Figure 7. Photovoltaic parameters of the devices, J-V characteristics under **(a)** dark and **(b)** light illumination (1 sun), **(c)** open circuit decay voltage diagram, and **(d)** electronic impedance spectroscopy curves.

(short circuit current density) Jsc of 0.88 mA cm^{-2}, (open circuit voltage) Voc of 0.43 V, and (fill factor) FF of 51.86%. In contrast, the nanohybrid-based devices demonstrated significant performance enhancements owing to the incorporation of carbon allotropes, which tune the electronic properties of NiO and improve its charge transport capabilities. Among these, the NM device exhibited the highest PCE of 0.80%, with a Jsc of 2.53 mA cm^{-2}, Voc of 0.56 V, and FF of 56.46%, followed by NF (0.72%), NR (0.60%), and NM (0.55%).

The observed improvements are primarily due to the synergistic interaction between NiO and the incorporated sp^2-hybridized carbon nanostructures. These allotropes offer enhanced electrical conductivity, accelerated electron transport, and reduced recombination losses by providing efficient charge migration pathways. Additionally, they raise the quasi-Fermi level of NiO, leading to increased Voc values. The increased surface area and the presence of additional active sites also promote superior dye loading and more efficient electron injection.

In particular, NM nanohybrid devices benefited from the high surface area of f-MWCNTs, forming a conductive network that facilitated rapid electron migration and higher dye adsorption. The performance of the NM-based DSSCs was further investigated by incorporating varying concentrations (10–50 wt%) of NM composite with TiO_2 as the base photoanode. The corresponding J–V profiles are shown in **Figure 7b**, and photovoltaic parameters are listed in **Table 2**.

While the bare TiO_2 device delivered a modest PCE of 4.85% (Jsc=11.35 mA cm^{-2}, Voc=0.63 V, FF=67.82%), significant improvements were observed with the addition of NM. The highest PCE of 6.50% was achieved with 20 wt% NM, along with a Jsc of 14.67 mA cm^{-2}, Voc of 0.67 V, and FF of 67.13%. Devices with 10%, 30%, 40%, and 50% NM showed PCEs

Table 2. Photovoltaic and electrochemical measurements.

Sample	Jsc (mA cm^{-2})	Voc (V)	PCE (%)	FF (%)	Rs (Ω)	Rrec (Ω)
NiO	0.88	0.43	0.17	51.86	39.42	48.11
NF	2.19	0.58	0.72	56.68	40.68	84.17
NM	2.53	0.56	0.80	56.46	47.87	90.94
NG	1.85	0.55	0.55	54.05	43.20	62.51
NR	1.91	0.54	0.60	58.17	44.78	65.34

of 5.72%, 5.88%, 5.62%, and 5.60%, respectively. The initial improvement is attributed to the optimized distribution of f-MWCNTs that promote fast electron transfer, suppress recombination, and increase dye adsorption. However, at higher concentrations (>20%), aggregation of f-MWCNTs likely hindered electron mobility and promoted recombination, leading to a slight decline in performance. These results highlight the importance of optimizing the NM content to balance charge transport and material dispersion.

To evaluate the stability of the devices, open-circuit voltage decay (OCVD) measurements were performed (**Figure 7c** and **Figure 8c**). Upon cessation of light exposure, a rapid decline in Voc followed by stabilization at low values was observed. This behavior indicates minimal back-electron transfer in the dark and confirms the favorable stability of the DSSCs.

To further probe internal charge transfer dynamics, EIS was conducted under dark conditions at 0.6 V bias (**Figures 7c** and **8d**). The Nyquist plots exhibited two prominent semicircles: the high-frequency arc corresponds to the charge transfer resistance (Rct) at the counter electrode/electrolyte interface while the mid- to low-frequency arc is assigned to the recombination resistance (Rrec) at the photoanode/

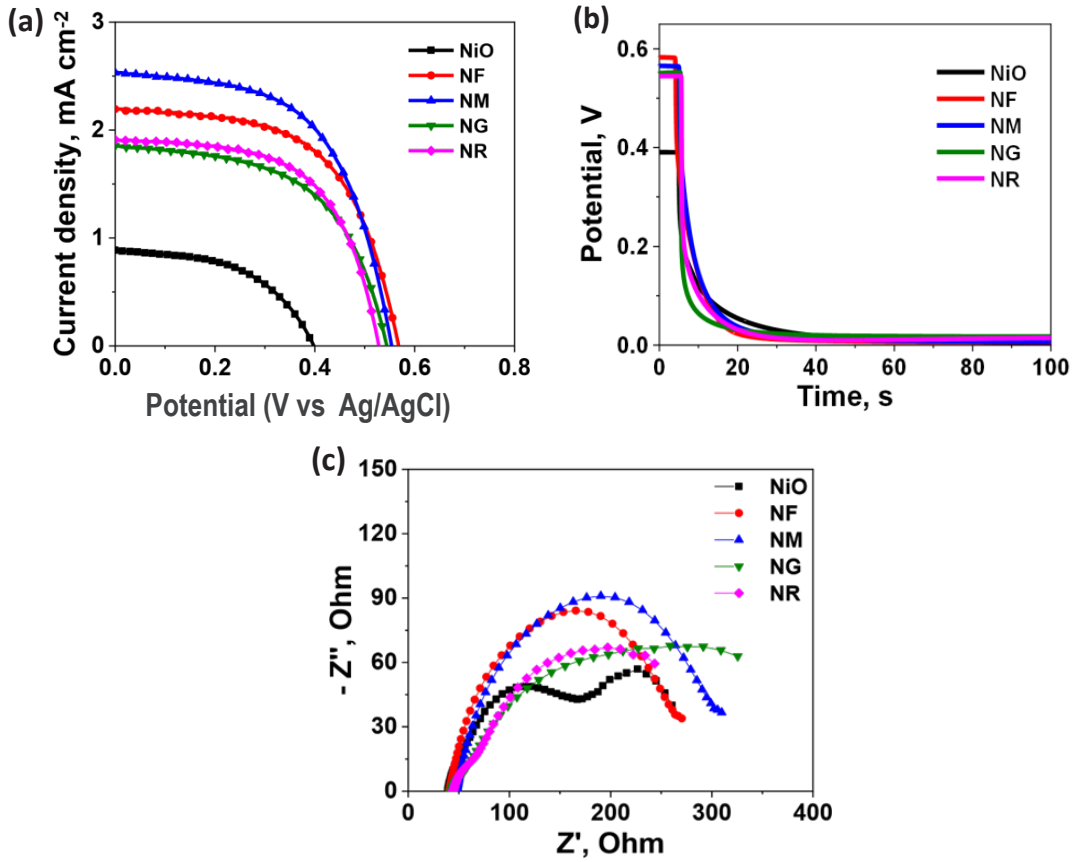

Figure 8. Photovoltaic characterization of DSSC devices, (**a**) J-V profile, (**b**) OCVD spectra, (**c**) EIS measurements.

electrolyte interface. An additional minor tail at low frequency represents Warburg impedance arising from ion diffusion in the electrolyte.

The EIS data in (**Table 1** and **2**) reveal that the reference TiO_2 device exhibited the lowest Rrec, implying high charge recombination and thus low photocurrent. In contrast, NM-based devices showed significantly higher Rrec values, particularly for the 20% NM composite, indicating suppressed recombination and efficient electron transport. The increased Rrec directly correlates with the high Jsc values observed. Lower Rct values in these devices also suggest better contact at the counter electrode/electrolyte interface.

In summary, the incorporation of NM nanocomposites into NiO and TiO_2 photoanodes markedly enhances the photovoltaic performance of DSSCs. These improvements stem from optimized electron transport, minimized recombination, increased dye adsorption, and favourable interfacial properties. Among all configurations, the 20% NM composite exhibited the best overall performance, validating its potential as a high-efficiency photoanode material for next-generation DSSCs.

Conclusion

The integration of carbon nanostructures with NiO nanotubes offers a compelling strategy for improving the efficiency of p-type DSSCs. This study systematically compared the performance of NiO hybrids with four different carbon allotropes f-MWCNTs, GQDs, RGO, and fullerenes revealing that NM exhibited the highest enhancement in photovoltaic parameters such as PCE, Jsc and FF 0.80%, 2.53 mA/cm^2 and 56.46% due to its superior charge transport and interfacial properties. Expanding on this, a ternary NiO/f-MWCNT/TiO_2 system was developed, demonstrating a significant improvement in power conversion efficiency PCE, Jsc 6.50%, 14.67. The incorporation of TiO_2 enabled better electron transport, while f-MWCNTs provided conductive pathways and facilitated efficient charge separation. These findings confirm that rational design of hybrid photoanodes combining p-type semiconductors with carbon nanomaterials and electron-conductive oxides can effectively address existing limitations in DSSC performance. This work not only contributes to the understanding of material interactions in hybrid photoanodes but also opens new avenues for the design of next-generation solar energy devices.

References

1. Anantharaj G, Lakshmi Narasimhan N. Interfacial Modification of Photoanode Electrolyte Interface Using Oleic Acid Enhancing the Efficiency of Dye-Sensitized Solar Cells. ACS Omega. 2018;3:18285–94.
2. Mehmood S, Ahmed U, Kumar L, Sagadevan S, Hatamvand M, Zhan Y, et al. Semiconducting metal oxides-based electrodes as the photoanodes of dye-sensitized solar cells (DSSCs). In: Pandey AK, Shahabuddin S, Ahmad MS, Editors. Dye-Sensitized Solar Cells. Emerging Trends and Advanced Applications. Cambridge, Massachusetts: Academic Press; 2022. pp. 103–36.
3. Perera IR, Daeneke T, Makuta S, Yu Z, Tachibana Y, Mishra A, et al. Application of the tris (acetylacetonato) iron (III)/(II) redox couple in p-type dye-sensitized solar cells. Angewandte Chemie International Edition. 2015 Mar 16; 54(12):3758-62.
4. Zinatloo-Ajabshir S, Salavati-Niasari M. Preparation of magnetically retrievable CoFe2O4@SiO2@Dy2Ce2O7 nanocomposites as novel photocatalyst for highly efficient degradation of organic contaminants Comp Part B: Engg. 2019;174: 106930.
5. Tsai CH, Lin CM, Liu YC. Increasing the efficiency of dye-sensitized solar cells by adding nickel oxide nanoparticles to titanium dioxide working electrodes. Coatings. 2020;10:1–13.
6. Prajapati N, Murthy CN, Machhi HK, Soni SS. A novel f-MWCNT-based nanocomposite for enhancement of photoconversion efficiency of DSSC. Journal of Materials Science: Materials in Electronics. 2023;34:2129.
7. Ko JW, Jeon S, Ko WB. Catalytic activity of nickel (II) oxide nanoparticle-[C60] fullerene nano whisker composite for reduction of 4-nitroaniline. Fullerenes, Nanotubes and Carbon Nanostructures. 2020;28:642–9.
8. Sharma N, Sharma V, Jain Y, Kumari M, Gupta R, Sharma SK, Sachdev K. Synthesis and characterization of graphene oxide (GO) and reduced graphene oxide (rGO) for gas sensing application. Macromolecular Symposia. 2017 Dec;376(1):1700006.
9. Al-bahrani MR, Liu L, Ahmad W, Tao J, Tu F, Cheng Z, Gao Y. NiO-NF/MWCNT nanocomposite catalyst as a counter electrode for high performance dye-sensitized solar cells. Applied Surface Science. 2015 Mar 15;331:333–8.
10. Subramanian A, Pan Z, Rong G, Li H, Zhou L, Li W, Qiu Y, Xu Y, Hou Y, Zheng Z, Zhang Y. Graphene quantum dot antennas for high efficiency Förster resonance energy transfer based dye-sensitized solar cells. Journal of Power Sources. 2017 Mar 1;343:39–46.
11. Yeoh ME, Chan KY. Recent advances in photo-anode for dye-sensitized solar cells: a review. International Journal of Energy Research. 2017;41:2446–67.
12. Ranganathan P, Sasikumar R, Chen SM, Rwei SP, Sireesha P. Enhanced photovoltaic performance of dye-sensitized solar cells based on nickel oxide supported on nitrogen-doped graphene nanocomposite as a photoanode. Journal of Colloid and Interface Science. 2017 Oct 15; 504:570–8.
13. Kumar YR, Deshmukh K, Ali MM, Abhijay G, Al-Onazi WA, Al-Mohaimeed AM, et al. Structure, morphology and modelling studies of polyvinylalcohol nanocomposites reinforced with nickel oxide nanoparticles and graphene quantum dots. Environmental Research. 2022 Jan 1; 203:111842.
14. Prajapati N, Sehgal P, Machhi H. Nickel oxide and carbon allotropes-based nanohybrids show enhanced efficiency of p-type dye-sensitized solar cells J Mater Sci: Mater Electron. 2025;36:870.

15. Wang TJ, Huang H, Wu XR, Yao HC, Li FM, Chen P, et al. Self-template synthesis of defect-rich NiO nanotubes as efficient electrocatalysts for methanol oxidation reaction. Nanoscale. 2019; 11(42):19783-90.

16. Nikita K, Ray D, Aswal VK, Murthy CN. Surface modification of functionalized multiwalled carbon nanotubes containing mixed matrix membrane using click chemistry. Journal of Membrane Science. 2020;596:11771.

17. Sehgal P, Narula AK. Enhanced performance of porphyrin sensitized solar cell based on graphene quantum dots decorated photoanodes. Optical Materials. 2018;79:435–45.

18. Meng Z-D, Zhu L, Choi J-G. Effect of Pt treated fullerene/TiO2 on the photocatalytic degradation of MO under visible light. J Mater Chem. 2011;21:7596–603.

19. Mistry B, Machhi HK, Vithalani RS, Patel DS, Modi CK, Prajapati M, et al. Harnessing the N-dopant ratio in carbon quantum dots for enhancing the power conversion efficiency of solar cells. Sustainable Energy and Fuels. 2019;3:3182–90.

20. Mihalache I, Radoi A, Mihaila M, Munteanu C, Marin A, Danila M, et al. Charge and energy transfer interplay in hybrid sensitized solar cells mediated by graphene quantum dots. Electrochimica Acta. 2015;153:306–15.

21. Singh R, Kaur N, Navjyoti, Mahajan A. Ni2+ enriched carbon nanotubes nanohybrids based non-platinum counter electrodes for dye sensitized solar cells. Solar Energy. 2021;226:31–9.